Site and orbital-dependent charge donation and spin manipulation in electron doped metal-phthalocyanines

Cornelius Krull[1], Roberto Robles[2], Aitor Mugarza[1*], Pietro Gambardella[1,3]

[1]*Catalan Institute of Nanotechnology (ICN), UAB Campus, E-08193 Barcelona, Spain*

[2]*Centre d'Investigacions en Nanociència i Nanotecnologia (CIN2), UAB Campus, E-08193 Barcelona, Spain*

[3]*Institució Catalana de Recerca i Estudis Avançats (ICREA) and Departament de Física, Universitat Autonoma de Barcelona, E-08193 Barcelona, Spain*

Abstract

Similar to silicon-based electronics, chemical doping offers a tool for tailoring the electrical characteristics of organic molecular compounds. Contrary to inorganic semiconductors, however, controlling the position of dopants and charge donation in molecular complexes is a complicated task due to the existence of multiple doping sites, electron acceptor levels, and intramolecular correlation effects. Here we use scanning tunneling microscopy to observe the position of single Li dopants within Cu-phthalocyanine and Ni-phthalocyanine molecules in contact with a metal substrate and probe the charge transfer process with unprecedented spatial resolution. We show that individual phthalocyanines can accommodate at least three stable nonequivalent doping sites and up to six dopant atoms. Ligand and metal orbitals can be selectively charged by modifying the configuration of the Li complexes. Because of strong charge-spin correlation in confined molecular orbitals, alkali atoms provide an effective way to tune the molecular spin without introducing magnetic dopants. Controlled manipulation of Li further shows that charge transfer is determined solely by dopants embedded in the molecules, whereas the magnitude of the conductance gap is sensitive to the molecule-dopant separation.

Electron doping of organic semiconductors constitutes an effective strategy for enhancing the performances of organic optoelectronic devices[1] and fabricating materials with exotic electronic properties,[2] such as organic superconductors[3,4] and Mott-Hubbard antiferromagnets.[5] In many cases, doping is achieved by the intercalation or co-deposition of alkali metals with molecular complexes, which can lead to dramatically increased conductivity,[6–8] better carrier injection efficiency from metal electrodes[9] and improved electroluminescent properties.[10] The family of metal-phthalocyanines (MPc), a class of macro-cyclic planar polyconjugated molecules, represents one of the best candidates to study the effects of chemical doping on organic systems and metal-organic contacts.[11–22] The great chemical stability and distinctive optical and electrical properties make them equally appreciated for technological applications, including organic field effect transistors,[23,24] light emitting devices,[10,25] and photovoltaic cells,[26] as well as for fundamental studies.[11–22]

Recent experiments reveal that multiple electron doping of MPc with alkali atoms leads to striking insulator−metal−insulator transitions as the molecular orbitals involved in the conduction go from being entirely empty to completely filled.[19,20] Moreover, the deposition of alkali species has been shown to improve both the spin injection efficiency[27] and spin coupling[28] between MPc and ferromagnetic metal layers. Photoemission and electron energy loss studies show that the filling pattern of MPc orbitals with either π- or *d*-character depends on the dopant concentration as well as on the central metal ion, highlighting the complexity of the doping process in metal-organic compounds.[11–17] Despite the increasing attention devoted to such systems, however, there is still no detailed description of the doping mechanisms at the single molecule level. Likewise, the interplay between dopants, molecules, and the conduction electron bath at a metal interface, which determines the low energy spectrum of the molecules and their conductivity, remains an open issue. As a metallic substrate can play the dual role of charge donor towards the molecules and acceptor for the dopants, this interplay needs to be addressed in detail.

Here, by performing scanning tunneling microscopy (STM) and spectroscopy (STS) experiments

and ab-initio electronic structure calculations, we investigate the charge transfer process in controlled doping sequences of CuPc and NiPc deposited on an Ag(100) substrate. We identify distinct doping sites, univocally relating the dopant position to the filling of specific molecular orbitals, and show that, depending on the doping configuration, a molecular charge (Q) and spin (S) of Q = 1 and 2 electrons, and S = 0, ½, can be obtained for a single donor atom. By manipulating Li atoms one-by-one, we show that a single molecule can accommodate up to six dopants. However, despite the fact that the doubly degenerate lowest occupied molecular orbital of CuPc and NiPc can be filled with up to four electrons in thick MPc films,[19,20] we find that charge transfer is limited to Q = 2 due to the presence of the metallic substrate. The latter acts as an electron sink to doped molecules, whereas it acts as electron donor to undoped species. Finally, we show that long-range electrostatic interactions can also affect the electronic structure of MPc, as Li adatoms located as far away as 3 nm from the center of the molecules modify the gap between the highest occupied and lowest unoccupied molecular orbitals.

Formation of Li_xMPc complexes

CuPc and NiPc molecules were deposited on a clean Ag(100) surface by thermal evaporation in ultra-high-vacuum. Doping was performed by dosing submonolayer amounts of Li at 5 K on the same surface. Figure 1a shows an STM image of Li atoms co-adsorbed with CuPc. The undoped molecules exhibit a typical four-leaf structure originating from the four isoindole ligands that form the aromatic Pc macrocycle. Each "leaf" presents a characteristic asymmetric intensity due to the rotation of the ligand axes relative to the high symmetry directions of the substrate, which gives rise to a chiral adsorption geometry.[29,30] The center appears as a depression due to the planar symmetry of the Cu^{2+} *d*-states near the Fermi level (E_F), which have a very low tunneling probability to the STM tip. Figure 1a reveals the presence of several molecules with distinct topographic features compared to CuPc, which we attribute to the spontaneous uptake of Li atoms. The most common

complexes, constituting more than 75 % of the total number of doped species, are those labeled LiCuPc-$\mathcal{L}_{\mathcal{A}}$ and LiCuPc-$\mathcal{M}$. The first type presents a bright double-lobe structure in correspondence of a benzene ring and a dark center. The LiCuPc-$\mathcal{M}$ type, on the other hand, presents a bright center and four symmetric ligands. The modified topography of the molecules can be directly associated to the position of the Li dopants on ligand and metal sites, respectively, as shown in the diagrams in Fig. 1b and c. Moreover, by manipulating the Li atom of a LiCuPc-$\mathcal{L}_{\mathcal{A}}$ complex with the tip of the STM, we find that a third stable doping site exists next to the aza-N atoms, which we label as LiCuPc-$\mathcal{L}_{\mathcal{B}}$ (Fig. 1c). These experimental findings are corroborated by density functional theory (DFT) calculations of several LiCuPc and LiNiPc bonding configurations (Fig. 2 and Supplementary Information). The configurations with the lowest adsorption energy of Li correspond to $\mathcal{L}_{\mathcal{A}}$, $\mathcal{L}_{\mathcal{B}}$, and $\mathcal{M}$. Furthermore, total energy calculations and STM topographic simulations suggest that the Li atom in the LiCuPc-$\mathcal{L}_{\mathcal{A}}$ complex is located between the benzene ring and the Ag surface rather than on top (Fig. 2 and Supplementary Fig. S3). Other configurations have also been observed in rare instances (Supplementary Fig. S1).

Selective electron and magnetic doping of molecular orbitals

The adsorption and electronic structure of CuPc and NiPc on Ag(100) has been extensively characterized in previous studies.[29–32] This allows us to focus on the effects of doping and, in particular, to correlate the dopant position to the charge transfer and distribution within the molecules. We performed differential conductance (dI/dV) measurements in order to probe the electronic structure of the different complexes, namely the local density of states at the position of the STM tip (see Methods for more details). We recall that undoped CuPc present a triplet ground state given by the coupling of the Cu spin ($S_{\mathcal{M}}$) to a ligand spin ($S_{\mathcal{L}}$) induced by charge transfer from

the substrate, which resides in a $2e_g$ orbital.[14] We refer to this state as having charge Q = 1 relative to gas-phase CuPc and total spin $S = S_{\mathcal{M}}+S_{\mathcal{L}} = 1$ (Fig. 3). The dI/dV spectra of CuPc reflect the single occupancy of the $2e_g$ orbital as one conductance peak below E_F, labeled "$2e_g$" in Fig. 3a, and its unoccupied counterpart "$2e_g$+U" above E_F, separated by the Coulomb energy U that corresponds to the energy cost of placing two electrons in the same orbital. Spatial maps of the dI/dV intensity, reported in Fig. 3b, confirm that the $2e_g$ and $2e_g$+U states have overlapping intensity and identical symmetry, as expected. At low temperature, the $2e_g$ ligand spin is screened by Ag electrons via the Kondo effect, which gives rise to the sharp resonance observed at E_F.

The doped species present a very different electronic structure compared to CuPc. We discuss first the case of Li attached to ligand sites, taking LiCuPc-$\mathcal{L}_{\mathcal{A}}$ as a representative example. Interestingly, all the $\mathcal{L}$-type configurations present very similar dI/dV spectra, leading to the conclusion, also supported by theory, that the charge transfer process is approximately the same in all the cases where Li dopants interact primarily with the aromatic Pc ring (Fig. 2c and Supplementary Fig. S1). The dI/dV spectrum of LiCuPc-$\mathcal{L}_{\mathcal{A}}$ reveals a multiple peaked structure below E_F, labeled α_{2eg}, and a shallow peak above E_F, labeled β_{2eg}. Unlike the $2e_g$ orbital in CuPc, spatial maps of the occupied α_{2eg} and unoccupied β_{2eg} features show two non-overlapping intensity profiles, each oriented along a single ligand axis (Fig. 3c). According to their symmetry, these orthogonal molecular orbitals originate from the splitting of the doubly degenerate $2e_g$ orbital of CuPc induced by Li. DFT calculations of the charge distribution confirm this assignment (Supplementary Fig. S2). The equally spaced multiple peaks observed for the α_{2eg} resonance correspond to vibronic excitations (see Supplementary Information), indicating partial decoupling of the doped complex from the substrate.[33] The vanishing intensity of the α_{2eg} peaks approaching E_F and the absence of its Coulomb pair above E_F indicate that the α_{2eg} orbital is fully occupied. With two electrons occupying one of the formerly degenerate $2e_g$ states of CuPc, LiCuPc-$\mathcal{L}_{\mathcal{A}}$ is thus doubly charged. Moreover, the pairing of

the electron spins in the α_{2eg} orbital leads to $S_{\mathcal{L}} = 0$, in agreement with the disappearance of the Kondo resonance at E_F (Fig. 3a). DFT calculations, on the other hand, show that the Cu spin remains unperturbed, as charge transfer is restricted to the α_{2eg} orbital (Supplementary Table I). Therefore, Li doping at ligand sites leads to a Q = 2, S = ½ configuration.

LiCuPc-$\mathcal{M}$ differs from both CuPc and LiCuPc-$\mathcal{L}_{\mathcal{A}}$. For this complex, a single peak is observed above E_F (Fig. 3a), which we assign to an unoccupied $2e_g$ resonance because of its four-fold symmetry about the ligand axes (Fig. 3d), similar to that of the unoccupied $2e_g$ states of CuPc. The additional intensity at the center is due to the presence of the Li atom at this site. The absence of occupied $2e_g$ peaks indicates that Li dopants at $\mathcal{M}$-sites inhibit electron transfer from the substrate to ligand orbitals, leading to $S_{\mathcal{L}} = 0$. Although STM provides no access to the Cu states near E_F,[30] our DFT calculations clearly show that Li transfers one electron to the b_{1g} orbital, the molecular state that originates from the hybridization of the Cu d_{x2-y2} and N $2p$ states, as shown by the spin-resolved projected density of states of LiCuPc-$\mathcal{M}$ compared to CuPc and LiCuPc-$\mathcal{L}_A$ (Fig. 2e). This leads to a nonmagnetic complex with Q = 1 and $S_{\mathcal{M}} = S_{\mathcal{L}} = 0$. Note that the larger charge transfer obtained by DFT (Fig. 2c and Supplementary Table SI) corresponds to an excess of charge in the $2e_g$ states arising from the well-known problem of treating correlation in delocalized orbitals with this method.[34] For the same reason, the splitting (U) of the singly and doubly occupied $2e_g$ states cannot be reproduced with accuracy by DFT.

Changing Ni for Cu and K for Li

MPc with different metal ions are believed to behave differently upon doping.[20] Here we investigate this effect by replacing NiPc with CuPc. This choice is motivated by the fact that, aside from the singlet ground state of the Ni^{2+} ion, the electronic structure as well as the substrate-induced charge transfer for the two species are very similar.[31] From the analysis of the STM images, we

observe that the $\mathcal{L}$–type position of the Li dopants is the same in NiPc and CuPc. However, $\mathcal{M}$–type species are rare and appear fuzzy at the center (Supplementary Fig. S1d), suggesting an unstable bonding configuration between Li and Ni atoms that can be easily perturbed by the STM tip. This fact can be qualitatively explained by the smaller electronegativity of Ni compared to Cu and is reflected also by the much larger binding energy computed for LiNiPc-$\mathcal{M}$ relative to the $\mathcal{L}$–species (Fig. 2b) as well as by the higher energy of the b_{1g} states of NiPc relative to CuPc (Fig. 2e). Figure 4 shows the dI/dV spectra and maps of NiPc, LiNiPc-$\mathcal{L}_{\mathcal{A}}$, and Li_2NiPc-$\mathcal{L}_{\mathcal{A}}$. The undoped molecule presents a spectrum that is very similar to CuPc, with a singly occupied $2e_g$ orbital below E_F, Kondo resonance, and unoccupied $2e_g$+U state. Charge transfer in LiNiPc-$\mathcal{L}_{\mathcal{A}}$, in contrast, differs significantly from LiCuPc-$\mathcal{L}_{\mathcal{A}}$ despite the equivalent position of the Li donor. The two sharp peaks that appear on either side of E_F (Fig. 4a) have both the symmetry of the α_{2eg} state (Fig. 4b). The orthogonal β_{2eg} state appears at higher positive bias and is thus fully unoccupied. Therefore, LiNiPc-$\mathcal{L}_{\mathcal{A}}$ has charge Q = 1 as opposed to Q = 2 of LiCuPc-$\mathcal{L}_{\mathcal{A}}$, where the α_{2eg} orbital is doubly occupied. This effect is attributed to the smaller electron affinity of the NiPc adsorbate, which is also reflected by the smaller uptake of charge estimated by DFT for NiPc relative to CuPc (Supplementary Table I). The absence of a Kondo resonance in LiNiPc-$\mathcal{L}_{\mathcal{A}}$ related to the unpaired α_{2eg} electron is consistent with the sharpness of the α_{2eg} peaks and the presence of vibronic satellites, indicating electronic decoupling from the substrate.

A Q = 2 state can be induced by doping LiNiPc-$\mathcal{L}_{\mathcal{A}}$ with an additional Li atom. The Li_2NiPc-$\mathcal{L}_{\mathcal{A}}$ complex has a fully occupied α_{2eg} orbital and a remarkably similar spectrum compared to that of singly doped LiCuPc-$\mathcal{L}_{\mathcal{A}}$ (Fig. 4a and c). This results in an equivalent electronic configuration of the Pc ring for these two species despite the fact that Li donors supply most of the excess charge in Li_2NiPc-$\mathcal{L}_{\mathcal{A}}$, whereas the Ag substrate contributes almost one electron to LiCuPc-$\mathcal{L}_{\mathcal{A}}$. Interestingly,

the same charge state can be reached by doping NiPc with a single K atom (Fig. 4a). This agrees with the intuitive concept that the heavy alkali metal atoms are more effective electron donors, even in the presence of the charge reservoir represented by the metallic substrate. Keeping in mind that Ni is diamagnetic in NiPc and that charge transfer to the metal orbitals is negligible for the $\mathcal{L}$–type complexes (Fig. 2c), the correlated charge and spin configurations of LiNiPc-$\mathcal{L}_{\mathcal{A}}$ and Li_2NiPc-$\mathcal{L}_{\mathcal{A}}$ correspond to Q = 1, S = ½, and Q = 2, S = 0, respectively.

Doping limit of single MPc

An important issue to optimize the doping process of organic semiconductors and metal-organic interfaces is the maximum number of dopants that can be hosted by a single molecule versus their combined effect in terms of amount of transferred charge and perturbation of the orbital energies. Evidently, the answer to this question depends on the type and size of each molecule. Nevertheless, the results presented here are relevant for the MPc family and reveal general trends for metal-organic interfaces that may be extrapolated to other systems. As seen in Fig. 1a and 4c, ligand sites can host more than one Li dopant. However, due to the low coverage of Li required by this study, the spontaneous formation of higher-doped species is extremely unlikely. We thus resorted to the STM manipulation of Li adsorbates in order to induce the formation of Li_xCuPc complexes atom-by-atom. A similar strategy, consisting in dragging the molecules over the dopants rather than vice versa, has been employed to investigate K-doped C_{60} complexes.[35] The complete manipulation sequence of Li_xCuPc is reported in the Supplementary Fig. S5. Figure 5a shows that CuPc with up to six Li dopants form stable Li_xCuPc complexes. We observe that the first complex formed in this way corresponds to LiCuPc-$\mathcal{L}_{\mathcal{A}}$, where the Li atom is attached to the benzene ring lying along the lateral approach direction of the STM tip. The second one corresponds to Li_2CuPc-$\mathcal{L}_{\mathcal{A}}$, with the additional

Li atom occupying the benzene site opposite to the first one. This appears to be the most stable double doping configuration, as we never observed complexes with Li atoms occupying adjacent benzene sites. Although the position of the additional dopants cannot be determined with high accuracy, also the third and subsequent dopants seem to prefer either benzene or pyrrole sites lying on the same axis and avoid empty rings adjacent to filled ones.

Figure 4b shows the dI/dV spectra as a function of the number of Li atoms. Remarkably, the absence of peaks crossing the Fermi level beyond $x = 1$ indicates that the charge transferred to the molecules saturates at Q = 2. This state, as mentioned before, is already reached in LiCuPc-$\mathcal{L}_{\mathcal{A}}$ with the filling of the α_{2eg} orbital with electrons coming from the substrate and a single Li dopant. The interaction with additional Li atoms affects only the energy of the α_{2eg} orbital, increasing the α_{2eg}-β_{2eg} energy gap (Fig. 5c) and inhibiting further charge transfer to the β_{2eg} state. The energy shifts of the α_{2eg} orbital is linear with x whereas the β_{2eg} energy remains approximately constant, which suggests that the Q = 2 state with all the dopants aligned along the same ligand axis is further stabilized by electrostatic interactions. As a consequence, we find a 100% increase of the gap, from 0.55 to 1.17 eV as measured using the onset of the peaks (Fig. 5c). Such strong variations due to local electrostatic interactions could play an important role in defining the homogeneity of the energy gap of doped organic semiconductor interfaces. Moreover, these results highlight differences and similarities between the doping of molecular crystals and metal-organic interfaces. On the one hand, the (lifting of degeneration and corresponding) energy gap opening at Q = 2 can explain the K_2MPc-K_4MPc phase separation observed in bulk-like films of FePc,[36] CuPc,[12] and ZnPc,[13] suggesting a stabilization plateau at Q = 2 common to MPc interfaced with metals as well as homogenous crystalline structures. On the other hand, the stabilization of the Q = 2 state seems to be much more significant at the metallic interface. Here the impossibility to induce higher charge states contrasts with the measurements of MPc bulk crystals, where a complete filling of the two-fold degenerate $2e_g$

orbital with Q = 4 occurs at high doping concentration.[11] A key element for such difference is the role of the metallic substrate, which appears to act as a charge sink limiting the MPc uptake of electrons to Q = 2. The tendency of grouping dopants along one ligand axis observed in Fig. 5a is consistent with the inhibition of charge transfer to the β_{2eg} orbital, which is located on the opposite axis.

Long-range interactions between dopants and molecules

Electron doping of organic semiconductor complexes is usually achieved by co-deposition or postdeposition of alkali metals without accurate control of the final position of the dopant atoms. This can result in local stoichiometry variations, posing the problem of how the electronic structure of a single molecule is affected by dopants that might, or might not, be attached to it. In general, we observe no uptake of charge unless the Li atoms are directly attached to the molecules. This explains why alkali metal levels of the order of one dopant per molecule or larger are required to induce appreciable conductivity changes in organic semiconductors.[3–8,20] Despite the absence of charging, however, we report sizeable electrostatic effects on the conductance gap induced by Li atoms in the vicinity of MPc. Figure 6 shows the result of a manipulation experiment where a Li atom is gradually approached to a LiNiPc-$\mathcal{L}_A$ complex from a distance r = 3 nm to contact (see inset). The conductance gap of LiNiPc-$\mathcal{L}_A$ corresponds to the separation between the singly (α_{2eg}) and doubly (α_{2eg}+U) occupied states, indicated by arrows in Fig. 6a. We find that the gap increases as the Li atom approaches the molecule (Fig. 6b), indicating that the excess charge induced by the Li atom to its surroundings affects the Coulomb repulsion of the molecular orbitals. Note that only the energy of the doubly occupied α_{2eg}+U orbital shifts in an appreciable way, suggesting that the higher charge state is more sensitive to Coulomb interactions. The spatial dependence is in line with the 1/r decay of the energy gap on a length scale of about 3 nm, which is similar to that reported for electrostatic

interactions of Li adatoms on Ag(100),[37] Cs superlattices on graphene,[38] and the lateral extension of charge densities induced by positive charges on metallic surfaces.[39] Such variations of the molecular orbital energies induced by proximity may be critical to reliably control electron injection and transport at metal-organic interfaces.[1,7,9]

Outlook

Understanding the interaction between molecules, dopants, and metallic interfaces with sub-molecular accuracy is key to the preparation of more efficient materials for organic optoelectronics.[1] Our results, which are free of the averaging effects typical of photoemission and transport studies, provide a detailed understanding of chemically doped metal-organic complexes. The competition between π- and *d*-like charge transfer channels and strong electron confinement make the doping of metal-organic molecules far more complicate compared to purely organic compounds.[35] However, as shown here, this complexity can be turned to an advantage and exploited to control the magnetism of the molecules, as the spin of either metal or ligand sites can be switched on or off by selectively doping different orbitals. Because the implementation of molecular spintronics relies on the ability to inject and manipulate charges and spins in metal-organic heterojunctions,[40] doped MPc provide an excellent example for promoting the use of doping beyond the realm of optoelectronics. Finally, the detection of single dopant properties in individual molecules and the ability to manipulate such dopants may be also envisioned as a first step for the realization of organic devices with magnetic and optoelectronic properties governed by ultimate discretization effects.[41]

METHODS

Sample preparation and STM measurements. CuPc and NiPc molecules were evaporated in ultra-high-vacuum on single crystal Ag(100). The substrate was prepared by repeated sputter-anneal cycles using Ar^+ ions at an energy of 700 eV and annealing to 800 K. The molecules were deposited

at a rate of ~0.05 monolayers/min with the sample kept at room temperature, after degassing the 99% pure powder material (Sigma Aldrich) to 500 K for 24 hours. The base pressure during evaporation was below 5×10^{-10} mbar. In a second step, the alkali metals were deposited in-situ at 4.8 K from SAES Getters sources. The STM measurements were carried out at the base temperature of 4.8 K. dI/dV spectra were measured using the lock-in technique, by modulating the bias voltage at a frequency of 3 kHz with rms amplitude of 3 mV. The dI/dV spectra are shown as measured, apart from that of NiPc (Fig. 4a), for which it was necessary to subtract a background spectrum acquired on the bare Ag surface with the same tip and feedback conditions in order to remove electronic features due to the substrate and tip. The dI/dV maps were measured at constant current using 10 mV rms bias modulation. The manipulation of Li atoms was carried out by 1) placing the STM tip on top of a single atom, 2) lowering the tunneling resistance down to 114-500 kΩ (V_b = -40 to -100 mV, I = 200 to 350 nA), and 3) laterally moving the tip at a speed of 20 Å/s to the target site.

Ab-initio calculations. The electronic structure of doped and undoped CuPc and NiPc molecules adsorbed on Ag(100) was calculated using the VASP implementation of DFT in the projector augmented plane-wave scheme. We used the local density approximation,[42,43] which has been shown to give reliable results for MPc adsorbed on metals.[30,31] We used a plane-wave cutoff of 300 eV. The calculated slab include 5 Ag atomic layers intercalated by 7 vacuum layers in the vertical direction, and a 7×7 lateral supercell. The positions of all atoms in the molecule and the first three Ag layers were relaxed vertically and laterally until forces were smaller than 0.05 eV/Å. Charge transfer and local magnetic moments were calculated using a Bader charge analysis.[44]

Author Information The authors declare no competing financial interests. Correspondence and requests for materials should be addressed to A.M. (aitor.mugarza@icn.cat).

Acknowledgements We thank N. Lorente and D. Sánchez-Portal for useful discussions. This work was supported by the European Research Council (StG 203239 NOMAD), Ministerio de Economía y Competitividad (MAT2010-15659), and Agència de Gestió d'Ajuts Universitaris i de Recerca (2009 SGR 695). A.M. acknlowledges the Spanish Ministerio de Ciencia e Innovación for a Ramon y Cajal Fellowship.

Author contributions C.K., A.M., and P.G. planned the experiment; C.K. and A.M. performed the

measurements; C.K., A.M., and P.G. analysed the data and wrote the manuscript. R.R. performed the DFT calculations. All authors discussed the results and commented on the manuscript.

References

1. Walzer, K., Maennig, B., Pfeiffer, M. & Leo, K. Highly Efficient Organic Devices Based on Electrically Doped Transport Layers. *Chem. Rev.* **107**, 1233–1271 (2007).

2. Tosatti, E., Fabrizio, M., Tóbik, J. & Santoro, G. Strong Correlations in Electron Doped Phthalocyanine Conductors Near Half Filling. *Phys. Rev. Lett.* **93**, (2004).

3. Hebard, A. F. *et al.* Superconductivity at 18 K in potassium-doped C60. *Nature* **350**, 600–601 (1991).

4. Mitsuhashi, R. *et al.* Superconductivity in alkali-metal-doped picene. *Nature* **464**, 76–79 (2010).

5. Takenobu, T., Muro, T., Iwasa, Y. & Mitani, T. Antiferromagnetism and Phase Diagram in Ammoniated Alkali Fulleride Salts. *Phys. Rev. Lett.* **85**, 381–384 (2000).

6. Haddon, R. C. *et al.* Conducting films of C60 and C70 by alkali-metal doping. *Nature* **350**, 320–322 (1991).

7. Parthasarathy, G., Shen, C., Kahn, A. & Forrest, S. R. Lithium doping of semiconducting organic charge transport materials. *J. Appl. Phys.* **89**, 4986–4992 (2001).

8. Minakata, T., Ozaki, M. & Imai, H. Conducting thin films of pentacene doped with alkaline metals. *J. Appl. Phys.* **74**, 1079–1082 (1993).

9. Kido, J. & Matsumoto, T. Bright organic electroluminescent devices having a metal-doped electron-injecting layer. *Appl. Phys. Lett.* **73**, 2866–2868 (1998).

10. Hung, L. S. & Tang, C. W. Interface engineering in preparation of organic surface-emitting diodes. *Appl. Phys. Lett.* **74**, 3209–3211 (1999).

11. Schwieger, T., Peisert, H., Golden, M., Knupfer, M. & Fink, J. Electronic structure of the organic semiconductor copper phthalocyanine and K-CuPc studied using photoemission spectroscopy. *Phys. Rev. B* **66**, (2002).

12. Flatz, K., Grobosch, M. & Knupfer, M. The electronic properties of potassium doped copper-phthalocyanine studied by electron energy-loss spectroscopy. *J. Chem. Phys.* **126**, 214702 (2007).

13. Giovanelli, L. *et al.* Phase separation in potassium-doped ZnPc thin films. *J. Chem. Phys.* **126**, 044709 (2007).

14. Evangelista, F. *et al.* Electronic Properties and Orbital-Filling Mechanism in Rb-Intercalated Copper Phthalocyanine. *J. Phys. Chem. C* **112**, 6509–6514 (2008).

15. Ding, H., Park, K., Green, K. & Gao, Y. Electronic structure modification of copper phthalocyanine (CuPc) induced by intensive Na doping. *Chem. Phys. Lett.* **454**, 229–232 (2008).

16. König, A., Roth, F., Kraus, R. & Knupfer, M. Electronic properties of potassium doped FePc from electron energy-loss spectroscopy. *J. Chem. Phys.* **130**, 214503 (2009).

17. Gargiani, P., Calabrese, A., Mariani, C. & Betti, M. G. Control of Electron Injection Barrier by Electron Doping of Metal Phthalocyanines. *J. Phys. Chem. C* **114**, 12258–12264 (2010).

18. Yan, L., Watkins, N. J., Zorba, S., Gao, Y. & Tang, C. W. Direct observation of Fermi-level pinning in Cs-doped CuPc film. *Appl. Phys. Lett.* **79**, 4148 (2001).

19. Craciun, M. F. *et al.* Electronic Transport through Electron-Doped Metal Phthalocyanine Materials. *Adv. Mater.* **18**, 320–324 (2006).

20. Craciun, M. F., Rogge, S. & Morpurgo, A. F. Correlation between Molecular Orbitals and Doping Dependence of the Electrical Conductivity in Electron-Doped Metal-Phthalocyanine Compounds. *J. Am. Chem. Soc.* **127**, 12210–12211 (2005).

21. Giovannetti, G., Brocks, G. & van den Brink, J. Ab initio electronic structure and correlations in pristine and potassium-doped molecular crystals of copper phthalocyanine. *Phys. Rev. B* **77**, 035133 (2008).

22. Filibian, M. *et al.* Strong Electronic Correlations in Li_{x}ZnPc Organic Metals. *Phys. Rev. Lett.* **100**, 117601 (2008).

23. Bao, Z., Lovinger, A. J. & Dodabalapur, A. Organic field-effect transistors with high mobility based on copper phthalocyanine. *Appl. Phys. Lett.* **69**, 3066–3068 (1996).

24. Boer, R. W. I. de *et al.* Ambipolar Cu- and Fe-phthalocyanine single-crystal field-effect transistors. *Appl. Phys. Lett.* **86**, 262109 (2005).

25. Parthasarathy, G., Burrows, P. E., Khalfin, V., Kozlov, V. G. & Forrest, S. R. A metal-free cathode for organic semiconductor devices. *Appl. Phys. Lett.* **72**, 2138–2140 (1998).

26. Singh, V. P. *et al.* Copper-phthalocyanine-based organic solar cells with high open-circuit voltage. *Appl. Phys. Lett.* **86**, 082106–082106–3 (2005).

27. Cinchetti, M. *et al.* Tailoring the Spin Functionality of a Hybrid Metal-Organic Interface by Means of Alkali-Metal Doping. *Phys. Rev. Lett.* **104**, 217602 (2010).

28. Lodi Rizzini, A. *et al.* Coupling Single Molecule Magnets to Ferromagnetic Substrates. *Phys. Rev. Lett.* **107**, 177205 (2011).

29. Mugarza, A. *et al.* Orbital Specific Chirality and Homochiral Self-Assembly of Achiral Molecules Induced by Charge Transfer and Spontaneous Symmetry Breaking. *Phys. Rev. Lett.* **105**, 115702 (2010).

30. Mugarza, A. *et al.* Electronic and magnetic properties of molecule-metal interfaces: Transition-metal phthalocyanines adsorbed on Ag(100). *Phys. Rev. B* **85**, 155437 (2012).

31. Mugarza, A. *et al.* Spin coupling and relaxation inside molecule–metal contacts. *Nat Commun* **2**, 490 (2011).

32. Stepanow, S. *et al.* Giant spin and orbital moment anisotropies of a Cu-phthalocyanine monolayer. *Phys. Rev. B* **82**, (2010).

33. Qiu, X. H., Nazin, G. V. & Ho, W. Vibronic States in Single Molecule Electron Transport. *Phys. Rev. Lett.* **92**, 206102 (2004).

34. Cohen, A. J., Mori-Sánchez, P. & Yang, W. Insights into Current Limitations of Density Functional Theory. *Science* **321**, 792–794 (2008).

35. Yamachika, R. Controlled Atomic Doping of a Single C60 Molecule. *Science* **304**, 281–284 (2004).

36. Roth, F., König, A., Kraus, R. & Knupfer, M. Potassium induced phase transition of FePc thin films. *J. Chem. Phys.* **128**, 194711 (2008).

37. Simic-Milosevic, V. *et al.* Substrate-mediated interaction and electron-induced diffusion of single lithium atoms on Ag(001). *Phys. Rev. B* **75**, 195416 (2007).

38. Song, C.-L. *et al.* Charge-Transfer-Induced Cesium Superlattices on Graphene. *Phys. Rev. Lett.* **108**, 156803 (2012).

39. Muiño, R. D., Sánchez-Portal, D., Silkin, V. M., Chulkov, E. V. & Echenique, P. M. Time-Dependent Electron Phenomena at Surfaces. *Proc. Natl. Acad. Sci. U.S.A.* **108**, 971–976 (2011).

40. Sanvito, S. Molecular spintronics. *Chem. Soc. Rev.* **40**, 3336 (2011).

41. Koenraad, P. M. & Flatté, M. E. Single dopants in semiconductors. *Nat. Mater.* **10**, 91–100 (2011).

42. Kresse, G. & Joubert, D. From ultrasoft pseudopotentials to the projector augmented-wave method. *Phys. Rev. B* **59**, 1758 (1999).

43. Kresse, G. & Furthmüller, J. Efficiency of ab-initio total energy calculations for metals and semiconductors using a plane-wave basis set. *Comp. Mater. Sci.* **6**, 15–50 (1996).

44. Tang, W., Sanville, E. & Henkelman, G. A grid-based Bader analysis algorithm without lattice bias. *J. Phys. Cond. Matter* **21**, 084204 (2009).

FIGURE CAPTIONS

Figure 1. Formation of Li_xCuPc complexes. **a,** STM topographic image of CuPc molecules and Li atoms co-deposited on Ag(100). The image size is 19.3 nm x 19.3 nm. Tunneling bias conditions: V_{bias} = -0.3 V, I_t = 0.17 nA. Green and red labels indicate doped molecules that formed spontaneously after Li deposition. Illustrative diagrams and close up STM images of different doping configurations: **b,** LiCuPc-$\mathcal{L}_{\mathcal{A}}$, **c,** LiCuPc-$\mathcal{L}_{\mathcal{B}}$, and **d,** LiCuPc-$\mathcal{M}$.

Figure 2. Calculated electronic structure of Li_xMPc complexes. a, Relaxed geometry calculated for different bonding configurations of LiCuPc. **b,** Total energy difference relative to the minimum energy configuration for the different configurations. **c,** Differential charge of the molecules and of the transition-metal (TM) ions relative to the gas-phase. **d,** Magnetic moment of the TM ions. **e,** Projected density of states of the undoped species, $\mathcal{L}_{\mathcal{A}}$, and $\mathcal{M}$ configurations.

Figure 3. Selective orbital doping of CuPc. a, dI/dV spectra taken on the benzene ring of CuPc, LiCuPc-$\mathcal{L}_{\mathcal{A}}$, and LiCuPc-$\mathcal{M}$. The setpoints are V_{bias} = -1 V, I =1 nA for LiCuPc-$\mathcal{L}_{\mathcal{A}}$ and LiCuPc-$\mathcal{M}$, and V_{bias} = -2 V, I = 3 nA for CuPc. A vertical offset has been added for clarity. Topographic images and dI/dV maps of **b,** CuPc, **c,** LiCuPc-$\mathcal{L}_{\mathcal{A}}$, and **d,** LiCuPc-$\mathcal{M}$ at the energies of the $2e_g$-related orbitals. Dashed arrows in the schematic orbital filling diagram correspond to the spin of pristine molecules, whereas solid arrows correspond to charge/spin transferred from substrate and dopant.

Figure 4. Doping of NiPc. **a,** dI/dV spectra taken on the benzene ring of NiPc and Li_xNiPc-$\mathcal{L}_{\mathcal{A}}$ complexes with x = 1, 2. A vertical offset has been added for clarity. The spectra of LiCuPc-$\mathcal{L}_{\mathcal{A}}$ and KNiPc-$\mathcal{L}_{\mathcal{A}}$ are shown for comparison with Li_2NiPc-$\mathcal{L}_{\mathcal{A}}$. Topographic image and dI/dV maps of **b,** LiNiPc-$\mathcal{L}_{\mathcal{A}}$ and **c,** Li_2NiPc-$\mathcal{L}_{\mathcal{A}}$. Note that a Li atom is adsorbed close to LiNiPc-$\mathcal{L}_{\mathcal{A}}$ in **b**, which does

not affect the conductance maps. Solid arrows in the schematic orbital filling diagram correspond to charge/spin transferred from substrate and dopant.

Figure 5. Atom-by-atom doping of CuPc. a, STM images showing the addition of up to 5 Li atoms to the same CuPc molecule. Size of top images: 4.7 nm x 4.7 nm; Size of center and bottom images: 3 nm x 3 nm. Each image is taken after a manipulation event where an additional Li atom is successfully bonded to the CuPc molecule (see Supplementary Information for more details). **b,** Corresponding dI/dV spectra of the Li_xCuPc complexes with $x = 0 – 6$. The spectra are taken on the bright benzene ring of each doped molecule with setpoint V_b = -1 V, I = 1 nA. **c,** Position of the α_{2eg} and β_{2eg} orbitals as a function of the number of Li dopants as determined by the onset of the peaks, indicated by ticks in **b**, and corresponding energy gap. The red line is a linear fit to the data. The error bar at $x = 3$ corresponds to gap values obtained for different dopant configurations (see Supplementary Fig. S5).

Figure 6. Long-range interactions between dopants and molecules. a, dI/dV spectra of a LiNiPc-$\mathcal{L}_{\mathcal{A}}$ complex with a second Li atom placed at a distance r = 1.2 and 1.7 Å from the center of the molecule (inset). Green and blue arrows indicate the position of the α_{2eg} and α_{2eg}+U orbitals, respectively. **b,** Energy of the occupied α_{2eg} and unoccupied α_{2eg}+U orbitals as a function of r and corresponding energy gap. The red line is a $1/r$ fit to the data.

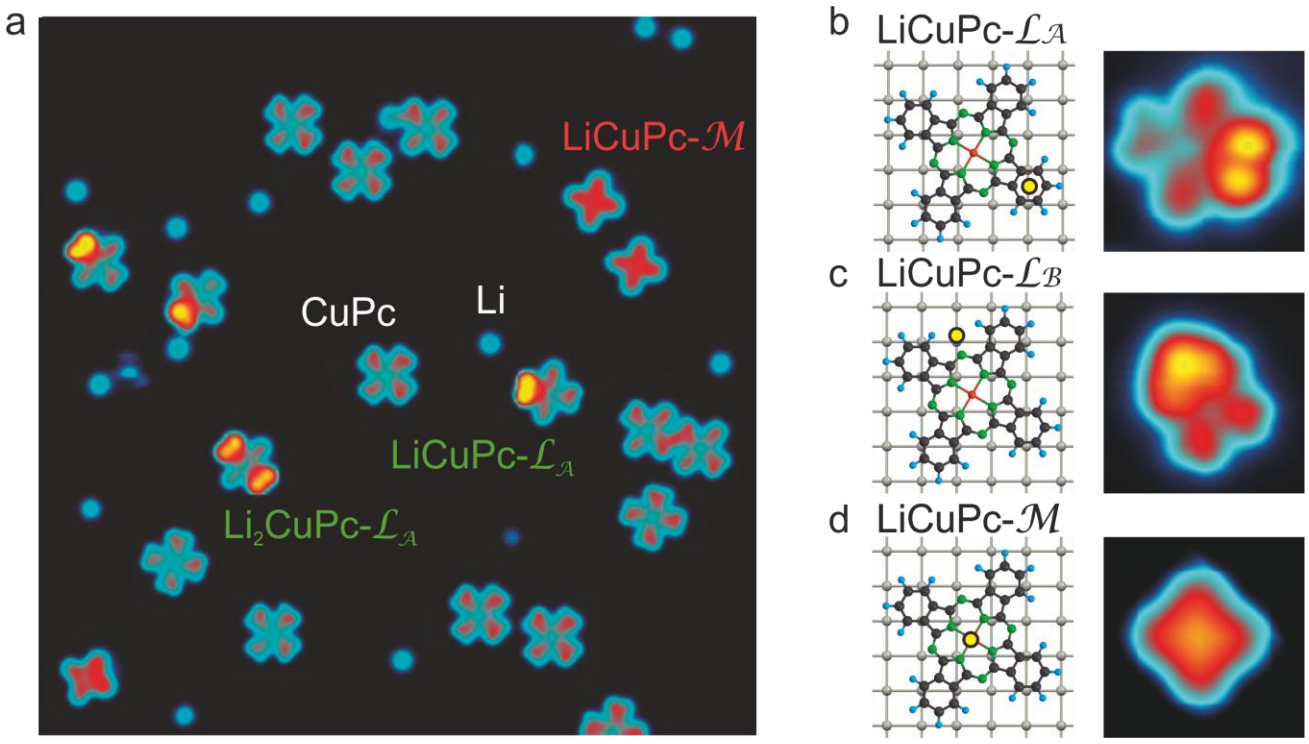
a
LiCuPc-$\mathcal{M}$
CuPc
Li
LiCuPc-$\mathcal{L}_{\mathcal{A}}$
Li_2CuPc-$\mathcal{L}_{\mathcal{A}}$
b
LiCuPc-$\mathcal{L}_{\mathcal{A}}$
c
LiCuPc-$\mathcal{L}_{\mathcal{B}}$
d
LiCuPc-$\mathcal{M}$

FIGURE 1

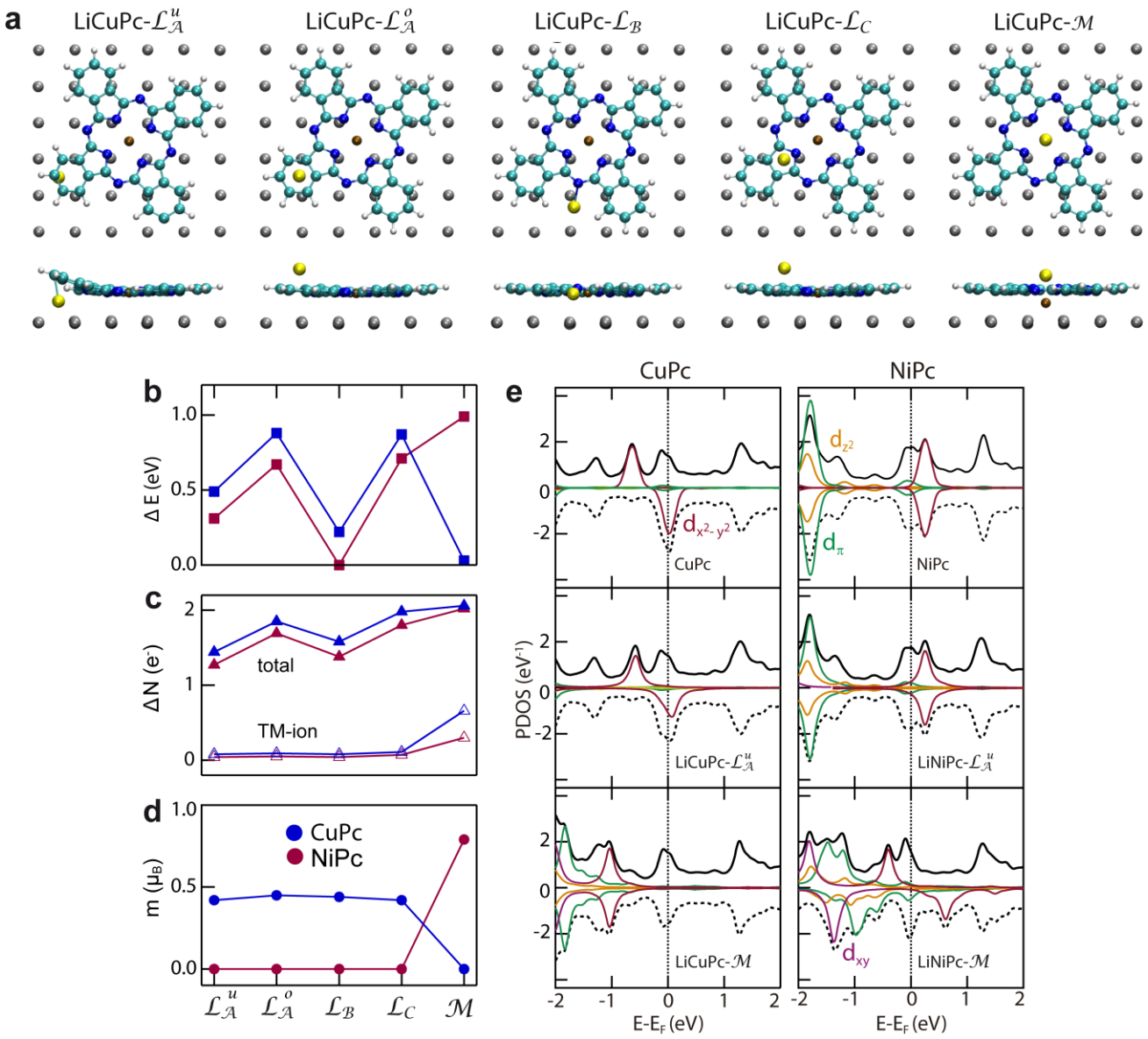
a
LiCuPc-$\mathcal{L}_{\mathcal{A}}^{u}$
LiCuPc-$\mathcal{L}_{\mathcal{A}}^{o}$
LiCuPc-$\mathcal{L}_{\mathcal{B}}$
LiCuPc-$\mathcal{L}_{C}$
LiCuPc-$\mathcal{M}$
b
Δ E (eV)
1.0
0.5
0.0
c
ΔN (e⁻)
2
1
0
total
TM-ion
d
m (μB)
1.0
0.5
0.0
CuPc
NiPc
$\mathcal{L}_{\mathcal{A}}^{u}$ $\mathcal{L}_{\mathcal{A}}^{o}$ $\mathcal{L}_{\mathcal{B}}$ $\mathcal{L}_{C}$ $\mathcal{M}$
e
CuPc
NiPc
PDOS (eV⁻¹)
$d_{x^2-y^2}$
CuPc
d_{z^2}
d_{π}
NiPc
LiCuPc-$\mathcal{L}_{\mathcal{A}}^{u}$
LiNiPc-$\mathcal{L}_{\mathcal{A}}^{u}$
LiCuPc-$\mathcal{M}$
d_{xy}
LiNiPc-$\mathcal{M}$
2
0
-2
-2 -1 0 1 2
E-E$_F$ (eV)

FIGURE 2

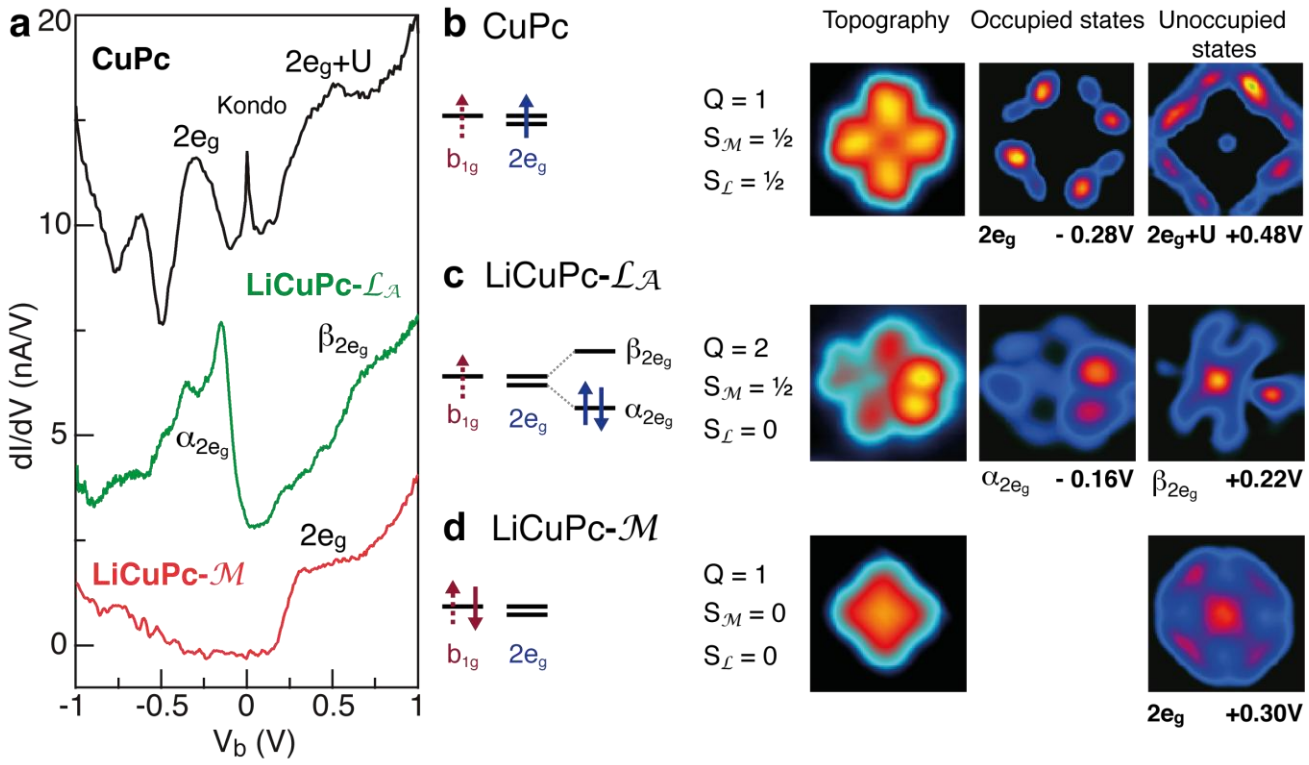
a
CuPc
2eg+U
Kondo
2eg
LiCuPc-$\mathcal{L}_\mathcal{A}$
β_{2e_g}
α_{2e_g}
2eg
LiCuPc-$\mathcal{M}$
dI/dV (nA/V)
Vb (V)
b CuPc
b1g
2eg
c LiCuPc-$\mathcal{L}_\mathcal{A}$
d LiCuPc-$\mathcal{M}$
Topography
Occupied states
Unoccupied states
Q = 1
$S_\mathcal{M}$ = ½
$S_\mathcal{L}$ = ½
2eg - 0.28V
2eg+U +0.48V
Q = 2
$S_\mathcal{M}$ = ½
$S_\mathcal{L}$ = 0
α_{2e_g} - 0.16V
β_{2e_g} +0.22V
Q = 1
$S_\mathcal{M}$ = 0
$S_\mathcal{L}$ = 0
2eg +0.30V

FIGURE 3

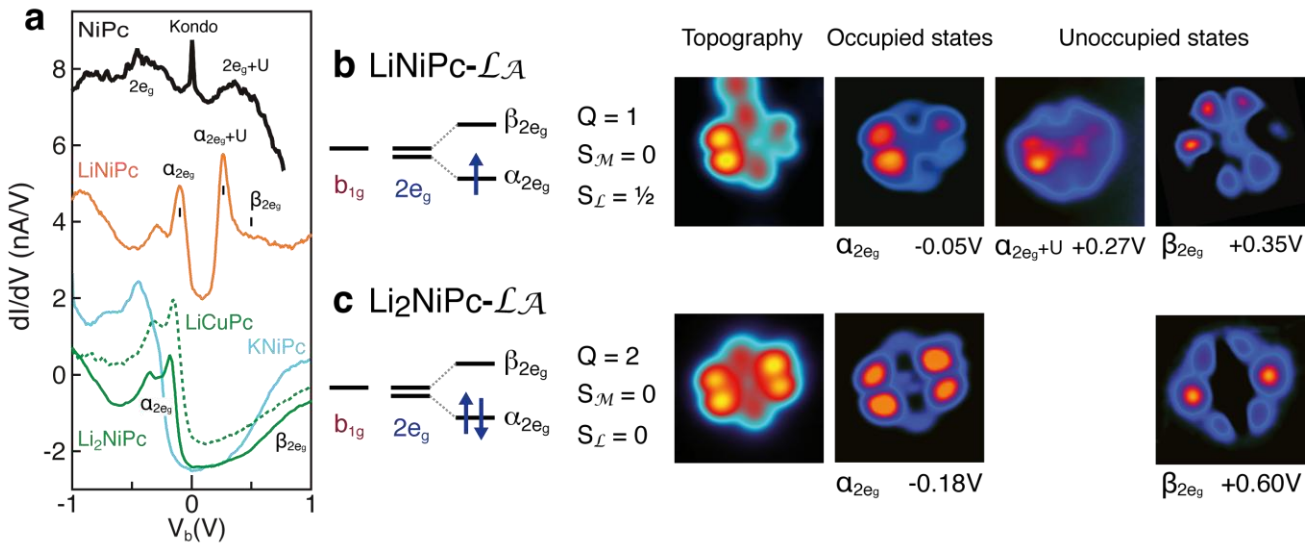
a
NiPc
Kondo
2e_g
2e_g+U
α_2e_g+U
LiNiPc
α_2e_g
β_2e_g
LiCuPc
KNiPc
α_2e_g
Li_2NiPc
β_2e_g
dI/dV (nA/V)
V_b(V)
b LiNiPc-ℒ𝒜
β_2e_g
α_2e_g
b_1g
2e_g
Q = 1
S_ℳ = 0
S_ℒ = ½
c Li_2NiPc-ℒ𝒜
β_2e_g
α_2e_g
b_1g
2e_g
Q = 2
S_ℳ = 0
S_ℒ = 0
Topography
Occupied states
Unoccupied states
α_2e_g -0.05V
α_2e_g+U +0.27V
β_2e_g +0.35V
α_2e_g -0.18V
β_2e_g +0.60V

FIGURE 4

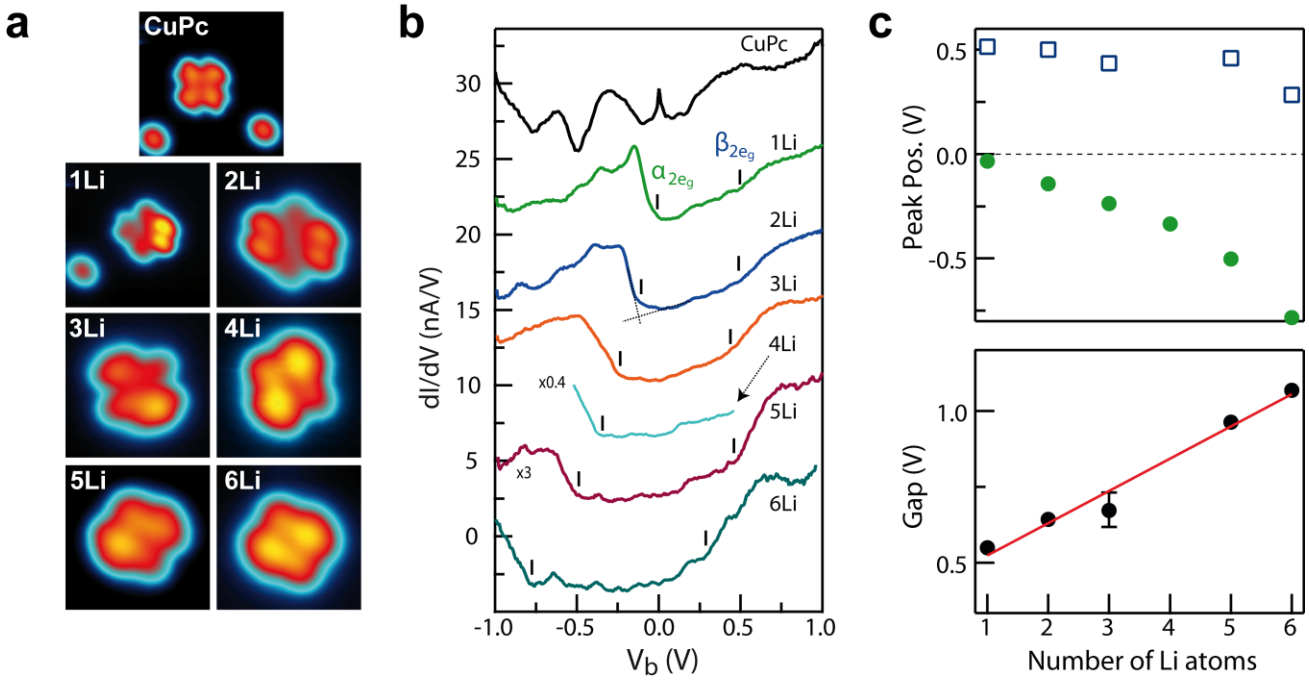
a
CuPc
1Li
2Li
3Li
4Li
5Li
6Li
b
CuPc
1Li
2Li
3Li
4Li
5Li
6Li
x0.4
x3
dI/dV (nA/V)
V_b (V)
c
Peak Pos. (V)
Gap (V)
Number of Li atoms

FIGURE 5

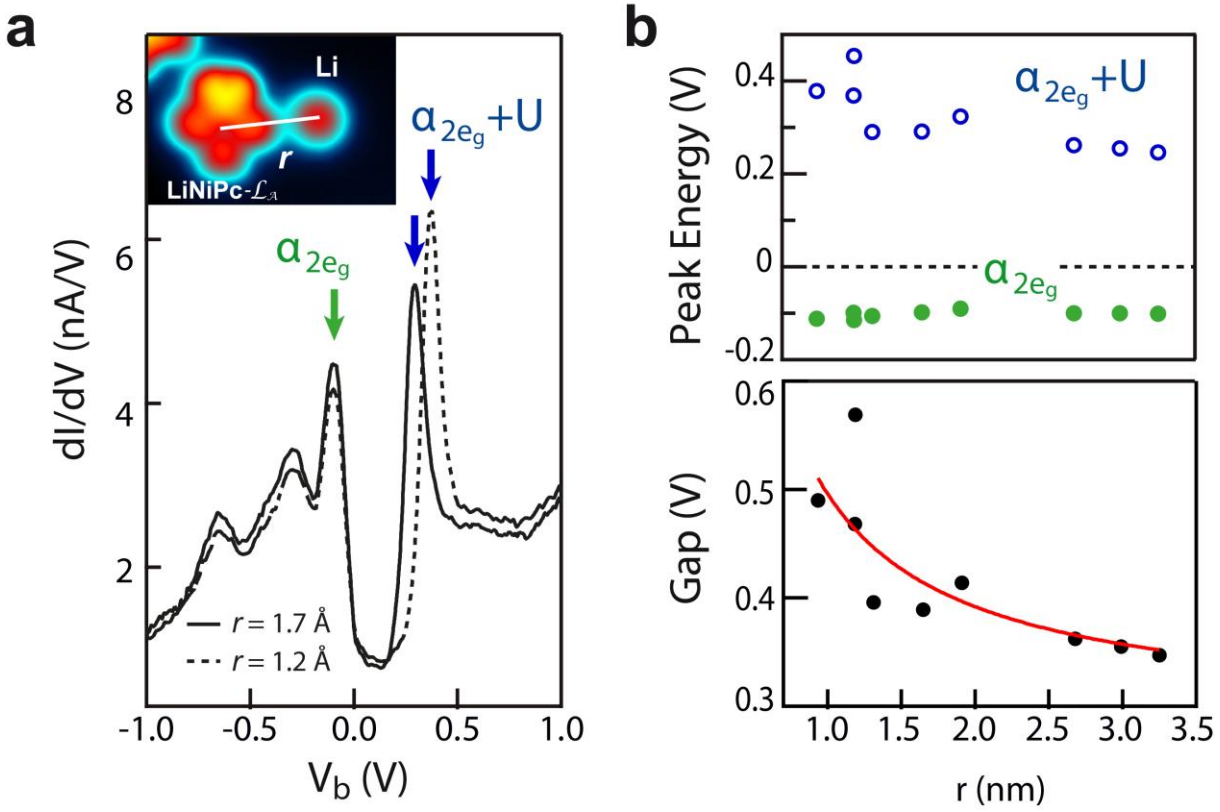
a
Li
r
LiNiPc-$\mathcal{L}_A$
α_{2e_g}+U
α_{2e_g}
r = 1.7 Å
r = 1.2 Å
dI/dV (nA/V)
V_b (V)
b
Peak Energy (V)
α_{2e_g}+U
α_{2e_g}
Gap (V)
r (nm)

FIGURE 6

Supplementary Information

Site and orbital-dependent charge donation and spin manipulation in electron doped metal-phthalocyanines

Cornelius Krull[1], Roberto Robles[2], Aitor Mugarza[1], Pietro Gambardella[1,3]

[1]*Catalan Institute of Nanotechnology (ICN), UAB Campus, E-08193 Barcelona, Spain*

[2]*Centre d'Investigacions en Nanociència i Nanotecnologia (CIN2), UAB Campus, E-08193 Barcelona, Spain*

[3]*Institució Catalana de Recerca i Estudis Avançats (ICREA) and Departament de Física, Universitat Autonoma de Barcelona, E-08193 Barcelona, Spain*

Contents

I. Rare LiMPc configurations

More than 75% of the observed LiMPc species correspond to the configurations $\mathcal{L}_{\mathcal{A}}$ and $\mathcal{M}$ described in the main text. In some instances, however, we observed different LiMPc configurations, which we report in Fig. S1. The first case (Fig. S1a) corresponds to a configuration obtained after manipulating a LiCuPc-$\mathcal{L}_{\mathcal{A}}$ species. After trying to push the Li atom away from the molecule, this remained bonded to the aza-N site, as can be observed in the topographic image. Such configuration corresponds to the LiCuPc-$\mathcal{L}_{\mathcal{B}}$ complex obtained by DFT (see Fig. 2a). Further attempts to separate this complex resulted in the diffusion of the whole molecule without changing the position of the Li atom relative to the Pc ring. This complex appears therefore to be stable and its electronic structure is very similar to LiCuPc-$\mathcal{L}_{\mathcal{A}}$, as revealed by the dI/dV spectra shown in Fig. S1a.

A second case is that of a LiCuPc complex with the ligand axes rotated by 45º with respect to the high symmetry directions of the substrate rather than the usual ±30º common to both undoped and doped molecules (Fig. S1b). A bright benzene ring is observed, indicating the presence of a Li ion similar to the LiCuPc-$\mathcal{L}_{\mathcal{A}}$ case. Here, however, the dI/dV spectrum is similar to that of LiNiPc-$\mathcal{L}_{\mathcal{A}}$, corresponding to a charge transfer of Q = 1, rather than LiCuPc-$\mathcal{L}_{\mathcal{A}}$ with Q = 2. After lateral manipulation of the complex, the configuration changes to that of the stable LiCuPc-$\mathcal{L}_{\mathcal{A}}$ configuration with Q = 2 (not shown).

A third configuration of doped CuPc complexes exhibits a bright protrusion which is laterally shifted from the center (Fig. S1c). The shift is of approximately 1 Å, as measured from the topographic profile of the image. The dI/dV spectrum is very similar to that of the stable LiCuPc-$\mathcal{M}$ species, indicating that charge transfer occurs through the *d*-states.

Finally, Fig. S1d shows an image of a fuzzy LiNiPc complex. The bright center and four-fold symmetry of the complex suggest that this is an $\mathcal{M}$–type configuration. The unstability of this

configuration, evidenced by the fuzziness of the image, is in full agreement with its large formation energy of about1 eV calculated by DFT for LiNiPc-$\mathcal{M}$ (see Table SI).

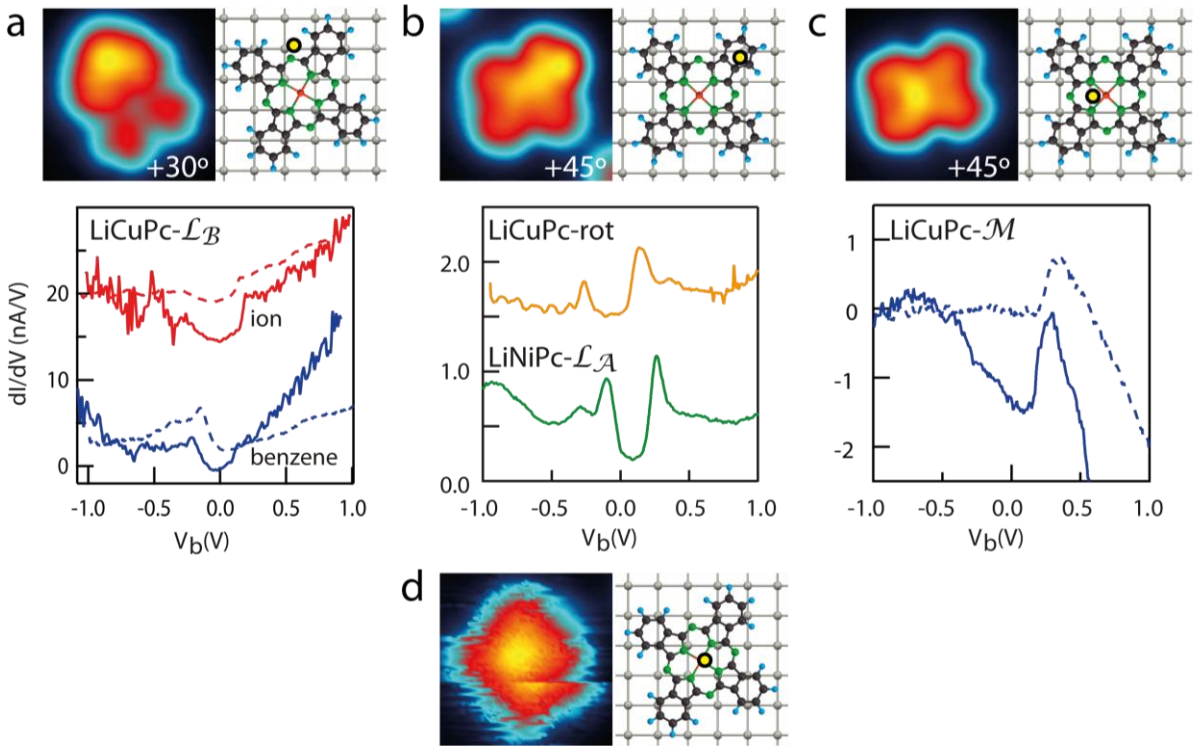

Figure S1. Rare LiMPc configurations. Topography (left), schematics (right), and dI/dV spectra (bottom) obtained for: **a**, LiCuPc-$\mathcal{L}_B$, with the Li bonded to the aza-N. Both dI/dV spectra measured on the Cu and benzene sites are very similar to those obtained for the $\mathcal{L}_A$ species (dashed lines). **b**, LiCuPc-$\mathcal{L}_A$ azimuthally rotated by +45º with respect to the high symmetry directions of the substrate. The spectrum is very similar to that of LiNiPc-$\mathcal{L}_A$, corresponding to a charge state for the $2e_g$ orbital of Q = 1. **c**, Asymmetric LiCuPc-$\mathcal{M}$, indicating that the Li ion is laterally shifted from the center of the molecule. The spectra is very similar to the symmetric case (dashed line) discussed in the text. A background spectrum acquired on Ag(100) has been subtracted to the data in this case in order to enhance molecular features. **d**, Unstable LiNiPc-$\mathcal{M}$. The fuzzy appearance is attributed to the unstability of the Li ion at the center. Spectroscopy could not be performed on this type of molecules.

II. DFT calculations

Charge density maps

In the ligand-doped molecules ($\mathcal{L}$) there is a clear correspondence between the position of the Li atom and the $2e_g$ acceptor level that shifts below the Fermi level. This is also evidenced by the charge density maps calculated by DFT (Fig. S2, left) of the formerly degenerate $2e_g$ orbital, which splits into a filled state localized along the axis containing the Li ion, and an empty state at higher energy along the orthogonal axis, as observed by STM. Note that empty states present an increased charge density at the Cu ion due to the energy overlap with the b_{1g} state (see Fig. 2e). In contrast, the $\mathcal{M}$ configuration (right) retains the four-fold symmetry of the doubly degenerate $2e_g$ state.

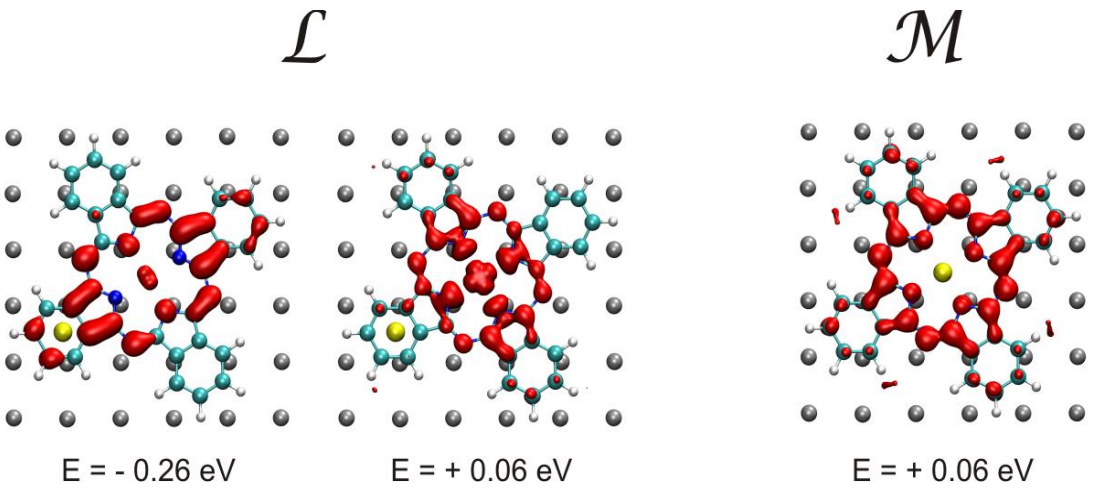

Figure S2. Charge density distribution of the $2e_g$ resonance of the $\mathcal{L}$ and $\mathcal{M}$ configurations of LiCuPc computed by DFT. The left panel shows the two orthogonal isocharge contours originating from the splitting of the $2e_g$ state for ligand-doped molecules. The right panel shows the four-fold symmetric contour of the $2e_g$ state for metal-doped species.

STM topographic images

Topographic images of LiCuPc complexes have been simulated using the Tersoff and Hamman theory[1,2] using the method of Ref. 3. A set of images obtained at -1.5 V for each configuration is displayed in Fig. S3. Comparison between the calculated and experimental images allows discriminating between different configurations. For example, in the case of the alkali adatom interacting with a benzene ring, only the $\mathcal{L}_{\mathcal{A}}{}^{u}$ configuration reproduces the double-lobe structure observed in the experimental images of the charged ring. This is also in agreement with the lower energy calculated for this configuration relative to $\mathcal{L}_{\mathcal{A}}{}^{o}$. Finally, the image calculated for the $\mathcal{M}$ configuration, with brighter intensity at the center, can be univocally associated to the doping of the metal site, consistently with the experimental results presented in the main text.

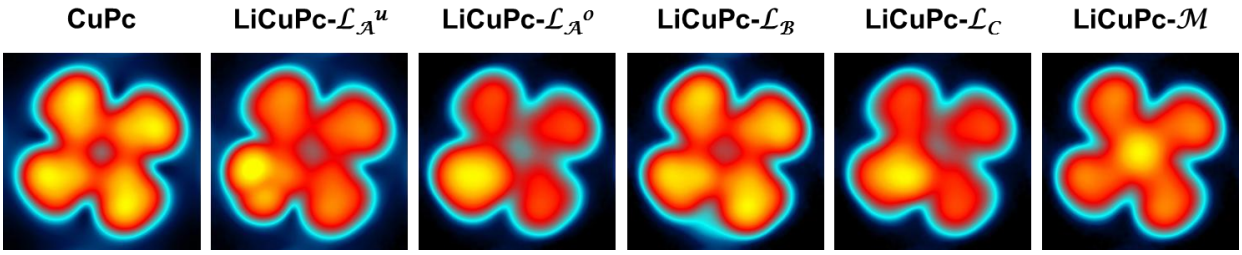

Figure S3. Topographic images of the different LiCuPc configurations computed by DFT. The images are obtained at V_{bias} = -1.5 V. The different features, such as the double-lobe structure and the bright center of the $\mathcal{L}_{\mathcal{A}}{}^{u}$ and the $\mathcal{M}$ configurations

Charge transfer, magnetic moment and total energy

The values for the total energy, magnetic moment and charge transfer displayed in Fig. 2 are listed in Table SI for the undoped and singly doped molecules. It can be noted that the total charge is higher than that derived from the experimental dI/dV spectra. This overestimation is related to the intrinsic difficulty of DFT in treating electron correlation, especially in highly delocalized orbitals such as the

$2e_g$ π-orbital.[4-6] For the same reason, the spin related to the presence of unpaired electrons in this orbital is missing in the calculations. As a consequence, we consider only quantitative values obtained for the transition-metal site (TM), related to the localized *d*-orbitals. The charge evolution in the $2e_g$ orbital is studied by following relative trends. For instance, the different charge states of the LiCuPc-$\mathcal{L}_{\mathcal{A}}^{u}$ and LiNiPc-$\mathcal{L}_{\mathcal{A}}^{u}$ complexes derived from the experimental data is reflected in the lower charge computed for the latter.

		ΔN (MPc)	ΔN (TM)	ΔN (Li)	ΔN (Ag)	m (TM)	ΔE
0 Li	CuPc	1.24	0.08	---	-1.24	0.45	---
	NiPc	1.07	0.04	---	-1.0	0.00	---
1 Li	$\mathcal{L}_{\mathcal{A}}^{u}$	1.44	0.08	-0.81	-0.63	0.42	0.46
		1.27	0.04	-0.81	-0.47	0.00	0.31
	$\mathcal{L}_{\mathcal{A}}^{o}$	1.85	0.09	-0.87	-0.98	0.45	0.85
		1.69	0.05	-0.87	-0.83	0.00	0.67
	$\mathcal{L}_{\mathcal{B}}$	1.58	0.08	-0.86	-0.73	0.44	0.19
		1.38	0.04	-0.89	-0.49	0.00	0.00
	$\mathcal{L}_{C}$	1.98	0.11	-0.87	-1.11	0.42	0.84
		1.80	0.07	-0.84	-0.96	0.00	0.71
	$\mathcal{M}$	2.06	0.66	-0.96	-1.10	0.00	0.00
		2.02	0.30	-0.89	-1.13	0.79	0.99

Table SI. Charge transfer, magnetic moment, and formation energies of doped LiMPc complexes calculated by DFT. Differential charge ΔN (in electron units) of the adsorbed molecules, transition metal ion (TM), Li ion, and Ag substrate relative to gas-phase MPc and unperturbed Ag surface. Magnetic moment m (in units of μ_B) of the metal ions. Relative formation energy ΔE (in eV). Rows corresponding to CuPc (NiPc) are grey (white). Note that, due to the hybridized $3d_{x2-y2}/2p$ character of the molecular b_{1g} orbital, the magnetic moment projected onto the metal ion captures only part of the S = ½ spin present in this orbital.

III. Vibronic excitations

Electrons tunneling to a molecular orbital having relatively large lifetime can inelastically excite vibrational states of the same orbital. This is often the case for molecules deposited on insulating layers, as the molecular orbitals hybridize only weakly with the substrate, which leads to an extended lifetime for the transient state. Such vibronic excitations will appear in dI/dV spectra as equidistant peaks overlaying the actual molecular orbital resonance.[7-9] The energy spacing is equal to the energy of the excited vibration. The detailed analysis of the peak structures found below the Fermi level for all LiMPc-$\mathcal{L}_{\mathcal{A}}$ complexes shows a series of equidistant peaks. The energy of the vibrational excitation is found to be between 173 and 193 meV. Literature values for the C-C and C-N stretching modes lie exactly within this energy range (150-200 meV).[10] Furthermore, PES measurements for thin films of CuPc on HOGP[10,11] and in the gas-phase[12] show a vibronic coupling of the HOMO of CuPc at the energy of 150 meV. We therefore interpret the multi-peak structure below E_F as a vibronic progression inside the molecules. Its presence indicates an increase of the electron lifetime within the molecules, and hence a Li-induced decoupling from the substrate.[7]

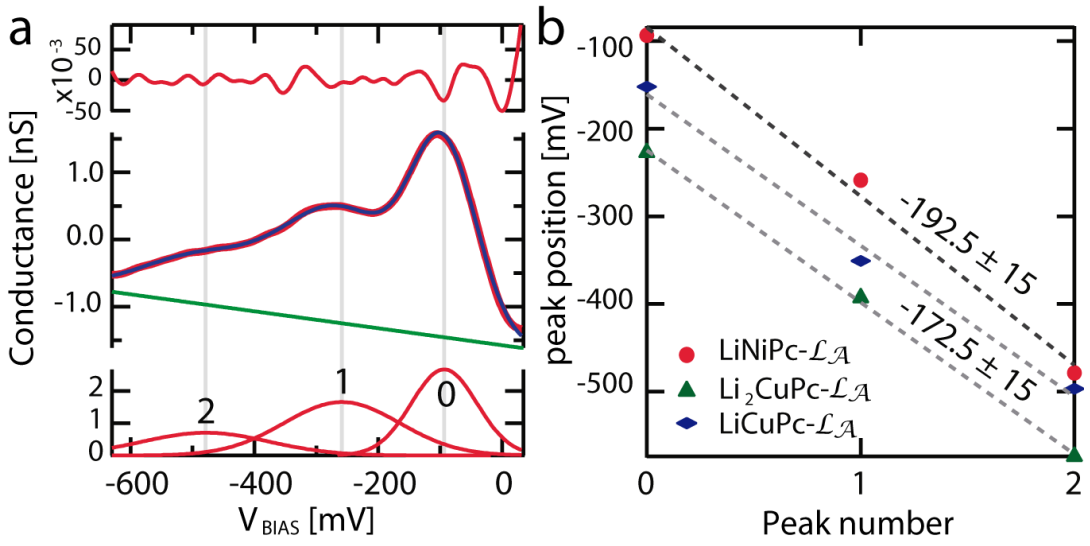

Figure S4. Vibronic coupling in $\mathcal{L}_{\mathcal{A}}$ species. Fitting of the vibronic satellite peaks with Lorentzian functions: **a**, Example of the fit obtained for the singly occupied $2e_g$ orbital in LiNiPc-$\mathcal{L}_{\mathcal{A}}$. **b**, The energy separation obtained for the multiple peaks is around 170 meV in both LiCuPc and Li_2CuPc species, and around 190 meV in LiNiPc.

IV. Atom-by-atom manipulation sequence

Although the LiMPc species form spontaneously by depositing Li atoms at low temperature, doping levels higher than one were rarely achieved due to the low coverage of Li required for the detailed study of individual molecules. Doping levels higher than two were studied for CuPc by using the STM tip to manipulate Li adsorbates. By laterally moving individual Li atoms one-by-one, up to six dopants could be introduced in the same molecule (see Methods for technical details). Figure S5 shows such a manipulation sequence including successful as well as failed doping attempts. We observed that dragging Li atoms towards the benzene rings yields $\mathcal{L}_{\mathcal{A}}$ configurations and that the molecules can rotate upon incorporation of dopants. We explored also the possibility of forming configurations with dopants occupying sites along the ligand axis orthogonal to that already occupied by other dopants. In such cases the molecule would rotate in order to incorporate the dopant in the same ligand axis (see doping with the 3rd Li atom in Fig. S5). dI/dV spectroscopy measurements carried out in between manipulation events were found to induce diffusion or rotation of metastable configurations. This resulted in an internal rearrangement of dopants, as shown in Fig. S4 for the case of Li_3CuPc. In this case the dopants could even be accommodated in orthogonal axes. However, this configuration proved particularly unstable, preventing us from performing spectroscopy measurements. The topography of the stable Li_4CuPc to Li_6CuPc configurations suggests accommodation of the Li atoms along the same ligand axis, consistently with the widening of the α_{2eg} - β_{2eg} gap observed in Fig. 5.

Figure S5. Atom-by-atom doping of CuPc induced by lateral manipulation of Li atoms. Arrows indicate the direction of the lateral motion of the tip between successive images.

V. Supplementary References

1. Tersoff, J., Hamann, D. R. Theory and Application for the Scanning Tunneling Microscope. *Phys. Rev. Lett.* **50**, 1998− 2001 (1983).

2. Tersoff, J., Hamann, D. R. Theory of the scanning tunneling microscope. *Phys. Rev. B* **31**, 805−813 (1985).

3. Bocquet, M.-L., Lesnard, H., Monturet, S., Lorente, N. In Computational Methods in Catalysis and Materials Science; van Santen, R. A., Sautet, P., Eds.; Wiley-VCH: Weinheim, Germany.

4. Mugarza, A. *et al.* Electronic and magnetic properties of molecule-metal interfaces: Transition-metal phthalocyanines adsorbed on Ag(100). *Phys. Rev. B* **85**, 155437 (2012).

5. Mugarza, A. *et al.* Spin coupling and relaxation inside molecule–metal contacts. *Nat Commun* **2**, 490 (2011).

6. Cohen, A. J., Mori-Sánchez, P. & Yang, W. Insights into Current Limitations of Density Functional Theory. *Science* **321**, 792–794 (2008).

7. Nazin, G. V., Wu, S. W., Ho, W. Tunneling rates in electron transport through double-barrier molecular junctions in a scanning tunneling microscope. *Proc. Natl. Acad. Sci. U.S.A.* **102**, 8832 – 8837 (2005).

8. Wu, S. W., Nazin, G. V., Chen, X., Qiu, X. H., Ho, W. Control of Relative Tunneling Rates in Single Molecule Bipolar Electron Transport. *Phys. Rev. Lett.* **93**, 236802 (2004).

9. Qiu, X. H., Nazin, G. V., Ho, W. Vibronic States in Single Molecule Electron Transport. *Phys. Rev. Lett.* **92**, 206102 (2004).

10. Kera, S., Yamane, H., Ueno, N. First-principles measurements of charge mobility in organic semiconductors: Valence hole–vibration coupling in organic ultrathin films. *Prog. Surf. Sci.* **84**, 135–154 (2009).

11. Kera, S., Yamane, H., Sakuragi, I., Okudaira, K. K., Ueno, N. Very narrow photoemission bandwidth of the highest occupied state in a copper-phthalocyanine monolayer. *Chem. Phys. Lett.* **364**, 93–98 (2002).

12. Evangelista, F. *et al.* Electronic structure of copper phthalocyanine: An experimental and theoretical study of occupied and unoccupied levels. *J. Chem. Phys.* **126**, 124709 (2007).